Energy & Environmental Science

ROYAL SOCIETY OF CHEMISTRY

PAPER

View Article Online
View Journal

Cite this: DOI: 10.1039/d5ee06413a

Effective mass model for thermoelectrics

Minsu Heo, †[ab] Kyu Hyoung Lee, †[c] Junwoo Song,†[d] Changwoo Lee,[b] Insub Lee,[d] Kwangjoo Kim,[d] Hoon Wee,[d] Joonhyun Lee,[d] Youngdeog Koh, *[d] Hyun-Sik Kim *[b] and G. Jeffrey Snyder *[a]

Thermoelectric materials require precise doping to adjust the Fermi level in order to fully realize their thermoelectric potential. The effective mass (EM) model is commonly used to predict the maximum thermoelectric figure-of-merit (zT) and optimal carrier concentration, but its application is limited by the need for numerical Fermi integral solutions and Hall effect measurements. Since the thermopower (magnitude of the Seebeck coefficient, $|S|$) is effectively a measure of the Fermi level, it can be used as a direct descriptor of doping level in heavily doped semiconductors such as good thermoelectric materials. Here, we present a simple method to analyze thermoelectric transport using only the typical thermoelectric measurements: Seebeck coefficient, electrical conductivity and thermal conductivity. This enables evaluation of weighted mobility, quality factor (B), theoretical maximum zT, optimal thermopower, identification of anomalous scattering behavior; as well as a full prediction of zT, as a function of $|S|$ given by

$$zT = \frac{\left(\frac{|S|}{k_B/e}\right)^2}{\left(\frac{1}{B}\right)\left[\frac{\exp\left[\frac{|S|}{k_B/e} - 2\right]}{1+\exp\left[-5\left(\frac{|S|}{k_B/e} - 1\right)\right]} + \frac{\frac{3}{\pi^2}\frac{|S|}{k_B/e}}{1+\exp\left[5\left(\frac{|S|}{k_B/e} - 1\right)\right]}\right] + (1.34)\left[1.5 + \exp\left(-\frac{|S|}{116\,\mu V\,K^{-1}}\right)\right]}$$

Received 27th October 2025,
Accepted 16th March 2026

DOI: 10.1039/d5ee06413a

rsc.li/ees

Broader context

Recent global energy analyses indicate that nearly 70% of all primary energy input is ultimately lost as waste heat during conversion and use, highlighting the urgent need for more efficient energy-conversion technologies. Thermoelectric materials can directly convert heat into electricity, offering a solid-state route to recover this wasted energy. However, optimizing their performance has long been hindered by the need for complex Fermi-integral calculations and Hall-effect carrier concentration measurements. These technical barriers have limited accurate thermoelectric analysis to a small fraction of the research community, even though thousands of studies each year report basic transport data such as Seebeck coefficient, electrical conductivity, and thermal conductivity. In this work, we reformulate the long-standing effective mass model into a simple and universal framework that allows any researcher to predict the maximum achievable figure-of-merit (zT) and its optimal carrier concentration directly from routine measurements, without numerical Fermi-integral analysis or Hall data. By transforming a specialized theoretical model into an experimentally accessible tool, this approach democratizes thermoelectric evaluation and accelerates the discovery of high-efficiency materials for waste-heat recovery and solid-state cooling, contributing to global efforts to enhance energy efficiency and achieve carbon-neutral technologies.

Introduction

Thermoelectric materials, capable of solid-state Peltier cooling and direct heat-to-electricity conversion, are drawing renewed interest as advances in electronic and phononic design continue to enhance performance. Electronic transport has improved from band engineering strategies that exploit complex Fermi surfaces, band convergence, and topological states,[1–5] while phonon transport has been suppressed through atomic-scale

[a] Department of Materials Science and Engineering, Northwestern University, Evanston 60208, IL, USA E-mail: jeff.snyder@northwestern.edu
[b] Department of Materials Science and Engineering, University of Seoul, Seoul 02504, Republic of Korea. E-mail: hyunsik.kim@uos.ac.kr
[c] Department of Materials Science and Engineering, Yonsei University, Seoul 03722, Republic of Korea
[d] Samsung Research, Samsung Electronics, Seoul 06765, Republic of Korea. E-mail: yd.koh@samsung.com
† These authors contributed equally to this work.

disorder and dislocation-induced strain.[6–9] These developments have expanded thermoelectric applications beyond refrigeration and waste heat recovery into emerging areas such as stretchable, body-heat-powered biosensors,[10] heat-triggered drug release and neuromodulation,[11] cryogenic quantum cooling using quantum dots,[12] and data center heat harvesting *via* hybrid thermoelectric systems.[13] As thermoelectrics become increasingly integrated into electronics, energy, and biomedical technologies, broadly applicable tools are needed to facilitate rapid analysis and optimization across both experimental and theoretical research fronts.

Most good thermoelectric materials behave as heavily doped semiconductors,[14–16] allowing semiempirical models from semiconductor physics to be used to explain, understand and then predict their thermoelectric performance. Despite the variety and complexity of thermoelectric materials, including both n-type and p-type compositions across structurally distinct classes such as rocksalt compounds (PbTe, SnTe), Zintl phases (Mg_3Sb_2), layered chalcogenides (Bi_2Te_3, BiCuSeO), skutterudites ($CoSb_3$), clathrates ($Ba_8Ga_{16}Ge_{30}$), half-Heuslers (FeNbSb), and complex silver chalcogenides (Ag_8SnSe_6), the effective mass (EM) model provides a consistent and predictive description of their electronic behavior. The model is also applicable to nanostructured materials,[17] to first-principles transport calculations using Boltzmann transport theory,[18] and to data-driven screening of new thermoelectric candidates using descriptors from materials databases, without requiring prior experimental characterization.[19] This demonstrates its utility as a unified approach for thermoelectric analysis. These results position the EM model as a unifying approach capable of capturing the essential physics of diverse and complex thermoelectric materials.

Although the model provides a simplified perspective, thermoelectric performance itself arises from a complex interplay among key transport properties. The complexity is due to the intricate interplay between the Seebeck coefficient (S), electrical conductivity (σ), and thermal conductivity (κ) that govern the thermoelectric figure-of-merit (zT), as shown in eqn (1):

$$zT = \frac{S^2\sigma}{\kappa}T \tag{1}$$

Achieving a high zT, reflecting superior thermoelectric performance, is not simply a matter of increasing S or even power factor ($S^2\sigma$), as these parameters are intrinsically coupled. In typical thermoelectric materials, not only do S and σ exhibit opposing trends with increasing carrier concentration, but κ includes an electronic contribution (κ_e) that varies with carrier concentration, in addition to the lattice component (κ_L) arising from phonon transport. The electronic trade-off for all three properties limits zT to a maximum at an optimal doping level (Fig. 1).

For effective optimization, one should use three largely independent variables instead of the interdependent S, σ, and κ which are achieved through the use of the weighted mobility, lattice thermal conductivity and a variable that quantifies the doping level. The weighted mobility, μ_w represents the quality

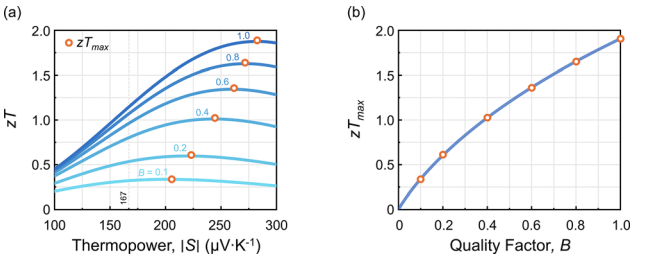

Fig. 1 Thermoelectric figure-of-merit (zT) change with carrier concentration tuning inferred from thermopower ($|S|$). (a) Plot of zT as a function of $|S|$, calculated using eqn (7). Changes in charge carrier concentration induced by doping are reflected in the corresponding $|S|$ values. The thermoelectric quality factor (B) determines the theoretical maximum zT (zT_{max}) achievable through carrier concentration optimization, with the optimal $|S|$ values to achieve zT_{max} indicated by orange circles. The $|S|$ corresponding to the maximum power factor (167 μV K^{-1}) is also indicated. (b) The zT_{max} values derived from different Bs in Fig. 1a are translated to a zT_{max} as a function of B relationship using eqn (S13).

of the electronic properties of a thermoelectric material system and the lattice thermal conductivity, κ_L represents the quality of the thermal properties. These two are combined into the thermoelectric quality factor, B, which determines the maximum zT, a material can achieve if optimally doped.

$$B = 0.674\left(\frac{T}{300\ \mathrm{K}}\right)^{5/2}\frac{\left(\frac{\mu_w}{1000\ \mathrm{cm^2\ V^{-1}\ s^{-1}}}\right)}{\left(\frac{\kappa_L}{\mathrm{W\ m^{-1}\ K^{-1}}}\right)} \tag{2}$$

The B equation (eqn (2)) is written such that the material targets for high performance become evident, with zT greater than 1 ($B > 0.4$) at room temperature typically requiring μ_w of about 500 cm^2 V^{-1} s^{-1} and κ_L less than 1 W m^{-1} K^{-1}.

Traditionally, carrier concentration (n) has been used as the third, largely independent variable to quantify doping. This stems from the original derivation of B based on ideal semiconductor assumptions, specifically the Single Parabolic Band model with acoustic phonon scattering (SPB-APS),[20,21] which later evolved into the EM model for broader applicability.[22] It is important not to conflate the effective mass used in the EM model with a strict definition from solid-state physics, such as the band curvature mass. Instead, it should be regarded as an effective parameter that fits measured or computed transport properties. Determining this parameter consistently for both degenerate and non-degenerate semiconductors, typically requires numerical solutions of Fermi integrals, which makes the EM model computationally intensive. The use of n, moreover, requires an additional measurement, typically Hall effect, which is often difficult or inaccurate in complex thermoelectric materials with low mobility.[23,24]

This work introduces a simplified yet robust model that does not require additional measurements or complicated calculations. It is based on the observation that the thermopower, the magnitude of the Seebeck coefficient $|S|$, is a reliable descriptor for n in thermoelectric materials and, like n, is largely insensitive to microstructure variations. Just as κ_e and μ_w can be calculated easily from thermoelectric measurements

of S and σ, we reformulate the zT equation as a function of $|S|$ alone (Fig. 1), with B ($\sim\mu_w/\kappa_L$) as the only required material parameter.[25,26] By preserving the essential physics of thermoelectric transport while eliminating the need for specialized measurements and complex calculations, our model enables rapid material screening and optimization. The approach provides clear design principles for advancing thermoelectric materials, making the field accessible to researchers across disciplines, both experimental and computational.

The EM model, based in semiconductor physics, explains the intrinsic trade-offs among S, σ and κ_e that fundamentally constrains zT. These transport parameters change with doping, which alters n. Although the Hall effect is typically used to characterize n, alternative descriptors can also capture doping effects. In particular, S and σ are especially sensitive to doping and can serve as practical proxies for n. When mobility (μ) is constant, σ is an obvious descriptor for n because $\sigma = ne\mu$ (where e is the electric charge). Indeed, plots of S *vs.* σ are helpful for optimizing thermoelectrics and identifying transport mechanisms[27,28] when μ is a constant or changes systematically.[29,30] However, the μ can change dramatically, for example with changing grain size when grain boundary scattering is significant.[26] Because the $|S|$, like the Hall coefficient is less affected by microstructure, $|S|$ is a better indicator of doping than σ for polycrystalline materials. $|S|$ is primarily determined by the Fermi level relative to the band edge, which is the same energy that determines how deep (in energy) the electrons have filled the bands and so also determines the number of free electrons n. The influence of scattering on S is relatively small and can be absorbed into the effective mass parameter.[14,31,32] This enables the Fermi level-dependent equations of the EM model,[22] such as κ_e, σ, and zT to be effectively re-expressed as a function of $|S|$ in degenerate semiconductors.

Using the Wiedemann–Franz law, $\kappa_e = L\sigma T$ (where L is Lorenz factor), both κ_e and κ_L can be determined from thermoelectric measurements of S, σ, and κ, using an L that depends on $|S|$. This approach is valid when bipolar conduction is negligible.[33,34]

$$L\left(\times 10^{-8}\,\mathrm{W\Omega K^{-2}}\right) = 1.5 + \exp\left(-\frac{|S|}{116\,\mu\mathrm{V\,K^{-1}}}\right) \tag{4}$$

with L estimated from eqn (4), the κ_L can then be obtained from eqn (3) ($\kappa_L = \kappa - L\sigma T$).

Weighted mobility

Weighted mobility μ_w, a crucial parameter in understanding electronic transport, can be accurately determined from S and σ measurements alone, eliminating the need for n data. This approach, expressed in eqn (5), is particularly valuable when only temperature-dependent S and σ data are available (where k_B represents the Boltzmann constant).[26]

$$\mu_w = 331\ \mathrm{cm^2\ V^{-1}\ s^{-1}}\left(\frac{\sigma}{\mathrm{m\Omega^{-1}\,cm^{-1}}}\right)\left(\frac{T}{300\,\mathrm{K}}\right)^{-3/2}\left[\frac{\exp\left[\frac{|S|}{k_B/e}-2\right]}{1+\exp\left[-5\left(\frac{|S|}{k_B/e}-1\right)\right]}+\frac{\frac{3}{\pi^2}\frac{|S|}{k_B/e}}{1+\exp\left[5\left(\frac{|S|}{k_B/e}-1\right)\right]}\right] \tag{5}$$

This method allows for facile determination of μ_w across a wide temperature range and remains accurate for $|S| > 20\ \mu\mathrm{V\ K^{-1}}$. Although originating from a free-electron treatment (parabolic band), it is employed here as an effective transport descriptor and remains applicable in systems with multi-band transport (Fig. S3).[35] For example, probing how μ_w *vs.* T, varies across samples, helps to determine whether differences arise purely from doping (μ_w remaining constant), or reflect more substantial underlying mechanisms. Within this formulation, μ_w captures nanostructure-induced changes in carrier transport, as variations in grain boundary scattering or interfacial effects manifest directly as shifts in μ_w, which thus integrates both electronic structure and microstructural contributions (see the SI).

Eqn (5) can be rearranged to examine how σ and therefore zT would change by improving μ_w.

$$\sigma = 3.02\ \Omega^{-1}\,\mathrm{cm^{-1}}\left(\frac{\mu_w}{\mathrm{cm^2\,V^{-1}\,s^{-1}}}\right)\left[\frac{\exp\left[\frac{|S|}{k_B/e}-2\right]}{1+\exp\left[-5\left(\frac{|S|}{k_B/e}-1\right)\right]}+\frac{\frac{3}{\pi^2}\frac{|S|}{k_B/e}}{1+\exp\left[5\left(\frac{|S|}{k_B/e}-1\right)\right]}\right]^{-1}\left(\frac{T}{300\,\mathrm{K}}\right)^{3/2} \tag{6}$$

Discussion

Electronic and lattice components to the thermal conductivity

$|S|$ has been successfully used to estimate the electronic contribution to thermal conductivity (κ_e) under the usual assumption that

$$\kappa = \kappa_e + \kappa_L \tag{3}$$

Figure of merit

With this arrangement, now both σ (eqn (6)) and κ_e (eqn (3) and (4)) are expressed in terms of thermopower, so zT can be written as a function of thermopower.

$$zT = \frac{\left(\frac{|S|}{k_B/e}\right)^2}{\left(\frac{1}{B}\right)\left[\frac{\exp\left[\frac{|S|}{k_B/e} - 2\right]}{1+\exp\left[-5\left(\frac{|S|}{k_B/e} - 1\right)\right]} + \frac{\frac{3}{\pi^2}\frac{|S|}{k_B/e}}{1+\exp\left[5\left(\frac{|S|}{k_B/e} - 1\right)\right]}\right] + (1.34)\left[1.5 + \exp\left(-\frac{|S|}{116\,\mu V\,K^{-1}}\right)\right]} \quad (7)$$

Eqn (7) is most reliable when diffusion thermopower dominates and bipolar effects remain limited.[36] In narrow band gap materials at elevated temperatures, the calculated zT should be regarded as an approximate descriptor. Further discussion is provided in the SI.

Then the only remaining material parameter in the zT equation is the thermoelectric quality factor B ($\sim\mu_w/\kappa_L$ in eqn (2)), alongside thermopower, which again describes the doping level.

Thermoelectric quality factor

As the B increases, the corresponding maximum zT (zT_{max}) also increases, reflecting the intrinsic quality of the material. Fig. 1a shows full zT curves as a function of thermopower ($|S|$) for various B values (eqn (7)), with the peak zT for each curve indicated by orange circles. This provides practical guidance for optimizing doping in materials with a known B. For example, a material with B = 0.4, which corresponds to a theoretical zT_{max} of 1.0, may only exhibit a zT of 0.8 at $|S|$ = 200 μV K^{-1}. Fig. 1a suggests that reducing the doping to increase $|S|$ to approximately 240 μV K^{-1} would enable the material to reach its theoretical zT_{max}, without requiring direct measurements of n.

Fig. 1b presents a direct correlation between B and the zT_{max}, constructed by mapping the peak points (orange circles) from Fig. 1a into a B-zT_{max} curve (Fig. 1b and Fig. S2). This relationship establishes clear performance targets. If a material's B falls below the threshold required for a target zT (*e.g.* B of 0.4 to achieve zT_{max} of 1.0), tuning the n alone will be insufficient. In such cases, alternative engineering strategies are required to enhance the B itself.

Effective mass

The namesake of the effective mass model is the effective mass, m^*, which is meant to be a material constant representing the density-of-states effective mass. In an ideal, parabolic, isotropic, single band system with acoustic phonon scattering, the various physics definitions of density-of-states effective mass will give the same value and remain constant with doping and temperature.[37,38] In contrast, the effective mass in real materials will vary with doping, temperature, and alloying, reflecting changes in band structure or dominant scattering mechanisms. Historically, in the EM model m^* is found using the Hall effect and thermopower where R_H is the Hall coefficient (m_e is the electron rest mass).[24]

Knowledge of m^*, and therefore the Hall-effect measurement is only needed to help distinguish electronic structure from scattering effects on electron transport. The analysis of thermoelectric data, including predicting and optimizing zT, does not require explicit knowledge of m^* and therefore does not require Hall effect measurements.

Example data analysis using EM model

Standard thermoelectric measurements of S, σ, and usually κ, can be easily used not only to analyze prospective zT, but also to gain insight into electronic structure, charge transport, and phonon behavior including an analysis of μ_w and κ_L.[39,40]

From the thermopower alone, one can assess whether a material would benefit from an increased or reduced doping. A high $|S|$ (>300 μV K^{-1}) is not an indicator of a good thermoelectric material, but instead points to underdoping (Fig. 1a), whereas a low $|S|$ (<200 μV K^{-1}) suggests that a reduced doping level to increase $|S|$ would be beneficial. Because the power factor peaks at ~167 μV K^{-1} irrespective of the material,[56] power factor-based optimization typically favors overdoped compositions (Fig. 2), leading to zT values up to ~25% below the theoretical zT_{max} (Fig. 1a, for B ~0.4) due to the neglected κ_e contribution. Even when power output is the primary objective rather than efficiency a thermoelectric device should maximize device ZT related to zT_{max}.[57,58]

The temperature dependence of $|S|$ provides key insight into whether the material is behaving as a metal, semiconductor, or insulator. $|S|$ proportional to T (measured in K) is characteristic of a metal or degenerate semiconductor, and indicates the parameters from the EM model are likely to represent intended materials properties (m^*, μ_w, and κ_L). At temperatures below 100 K the EM model parameters can be difficult to interpret due to physical effects such as phonon-drag thermopower, electron localization, or related phenomena.[59,60]

Whereas $|S|$ decreasing with T indicates the onset of bipolar conduction involving both electrons and holes like an insulator or non-degenerate (intrinsic) semiconductor. If temperature-dependent $|S|$ exhibits a maximum, the peak value ($|S|_{max}$) and the temperature at which it occurs (T_{max}) can be used to estimate the thermal band gap as $E_g = 2|S|_{max}T_{max}$. Care must be taken when predicting zT at temperatures above T_{max}, since a B estimated in the presence of bipolar conduction will be underestimated due to its influence on S and the additional bipolar contribution included in κ_L.[61,62]

$$\frac{m^*}{m_e} = 0.924\left[\frac{1/(eR_H)}{10^{20}\,cm^{-3}}\right]^{2/3}\left[\frac{3\left(\exp\left[\frac{|S|}{k_B/e} - 2\right] - 0.17\right)^{2/3}}{1+\exp\left[-5\left(\frac{|S|}{k_B/e} - \frac{k_B/e}{|S|}\right)\right]} + \frac{\frac{|S|}{k_B/e}}{1+\exp\left[5\left(\frac{|S|}{k_B/e} - \frac{k_B/e}{|S|}\right)\right]}\right]^{-1}\left(\frac{300\,K}{T}\right) \quad (8)$$

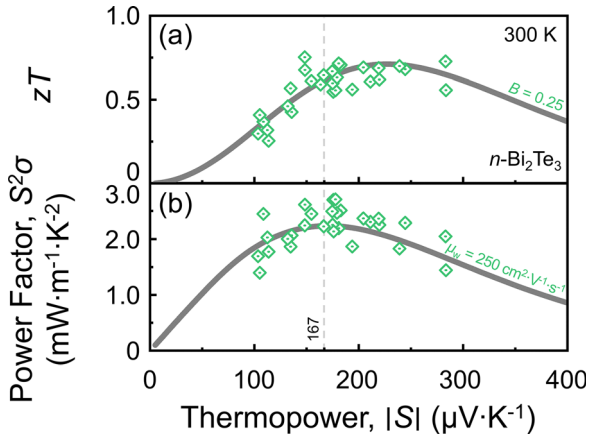

Fig. 2 Thermopower optimization for the best thermoelectric performance. Thermopower ($|S|$)-dependent (a) figure-of-merit (zT) and (b) power factor ($S^2\sigma$) for n-type Bi_2Te_3 at 300 K. While $|S|$ ~167 μV K^{-1} is the optimum value for the power factor across all materials, for zT this $|S|$ corresponds to an overdoped composition.[41–55]

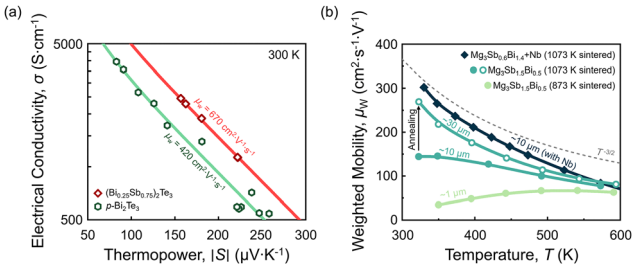

Fig. 3 Changes in electronic structure and carrier scattering revealed through weighted mobility (μ_w). (a) μ_w of $(Bi_{0.25}Sb_{0.75})_2Te_3$ and Bi_2Te_3 estimated using eqn (6). Band convergence in $(Bi_{0.25}Sb_{0.75})_2Te_3$ is reflected as an increase in μ_w relative to Bi_2Te_3.[63–72] (b) Grain boundary scattering associated with grain size is observed in $Mg_3(Sb,Bi)_2$.[73,74] Segregation of Nb to grain boundaries reduces potential barrier and enhances μ_w.[74]

With just S and σ, the μ_w can be readily evaluated using eqn (5). Its magnitude alone provides a first-order estimate of a material's suitability for thermoelectric applications. Eqn (2) indicates that a μ_w of approximately 600 $cm^2\ V^{-1}\ s^{-1}$ is required to achieve $B \sim 0.4$, corresponding to $zT_{max} \sim 1$ at 300 K in a material with $\kappa_L \sim 1\ W\ m^{-1}\ K^{-1}$.

Since μ_w can be directly calculated from experimental quantities, it can be presented as a better indicator of electronic performance than power factor, though caution should be taken against interpreting it as a single-band mobility.

The temperature dependence of μ_w is a sensitive probe of the dominant carrier scattering mechanism. A decrease in μ_w with increasing T indicates that thermal vibrations (phonons) dominate carrier scattering (eqn (5)). In both degenerate (metal-like) and non-degenerate semiconductors, μ_w typically follows a $T^{-3/2}$ trend, whereas in metals σ scales as T^{-1}.[75]

The variation of $|S|$ and σ across multiple samples can be analyzed through the μ_w to determine whether differences arise solely from doping or defects, or from more fundamental changes in transport. At a fixed temperature, μ_w can be treated as a fitting parameter and $|S|$ as the independent variable in eqn (5) to fit multiple data points. If the variation in μ_w is within ~20%, greater relative differences in S and σ are likely due to variation in doping or defect levels.

For example, $(Bi_{0.25}Sb_{0.75})_2Te_3$ samples in Fig. 3a doped with excess Te all exhibit similar μ_w (~670 $cm^2\ V^{-1}\ s^{-1}$). However, μ_w of $(Bi_{0.25}Sb_{0.75})_2Te_3$ is over 50% higher than that of Bi_2Te_3. This increase reflects band convergence at the 25% Bi_2Te_3-75% Sb_2Te_3 composition, which enhances the density-of-states effective mass (m_d^*). This m_d^* enhancement, in turn, drives the observed μ_w increase, since μ_w is mobility-weighted by the density of electronic states and follows $\mu_w \propto \mu(m_d^*/m_e)^{3/2}$.

Large deviations in μ_w often indicate changes in carrier scattering, such as additional grain boundary scattering, which can frequently be identified from its temperature dependence (Fig. 3b). An increase in μ_w with T indicates non-phonon scattering ($Mg_3(Sb,Bi)_2$ sample with ~1 μm grain size), primarily from electrical resistance at grain boundaries. Because this scattering diminishes as grain size increases from 1 μm to 30 μm, it can be attributed to grain boundary rather than ionized impurity scattering. Near room temperature, enlarging the grain size of $Mg_3(Sb, Bi)_2$ from 1 μm to 30 μm reduces the number of grain boundaries encountered by carriers and increases μ_w. In Nb-doped $Mg_3(Sb,Bi)_2$, where Nb segregates to grain boundaries, μ_w is even higher than in the 30 μm sample despite a grain size of only 10 μm, owing to the suppression of grain boundary potential barriers by Nb.

In systems deviating from ideal single-band or parabolic behavior, μ_w should be interpreted as an effective transport descriptor rather than a strict band parameter, and its primary strength lies in comparative analysis.

This transport-level perspective can also be extended to organic thermoelectrics, where transport is often influenced by structural disorder. Although eqn (7) achieves its highest quantitative reliability in band-like regimes, the weighted mobility μ_w extracted from the S–σ relationship remains informative for assessing the extent to which conduction is limited by disorder.[28,30]

Predicting zT_{max} and determining the optimum $|S|$ to achieve it is a primary role of the EM model, and eqn (7) alone can replace the full EM model for this purpose. Fig. 4 presents both experimental and theoretical n-dependent zT, converted into thermopower-dependent zT using eqn (7). In 2011, Böttger *et al.* reported a zT of 0.36 for Cu-doped ZnSb with $n = 5 \times 10^{18}$ cm^{-3}, and predicted that increasing n to 2×10^{19} cm^{-3} would raise zT to 0.45.[76] A decade later, Sn doping in the Zn-rich ZnSb phase space further increased n close to 2×10^{19} cm^{-3} and achieved $zT = 0.43$, close to the 2011 prediction.[77] In 2013, Day *et al.* predicted that decreasing doping in Ag_2Se could, in theory, yield $zT \sim 1.1$. Despite significant efforts to reduce doping, the optimum $|S|$ for achieving zT_{max} has not yet been reached.[79–84]

By reformulating the EM model in terms of thermopower and the thermoelectric quality factor, this work distils the essential physics of thermoelectric optimization into a form accessible from routine measurements. The approach enables

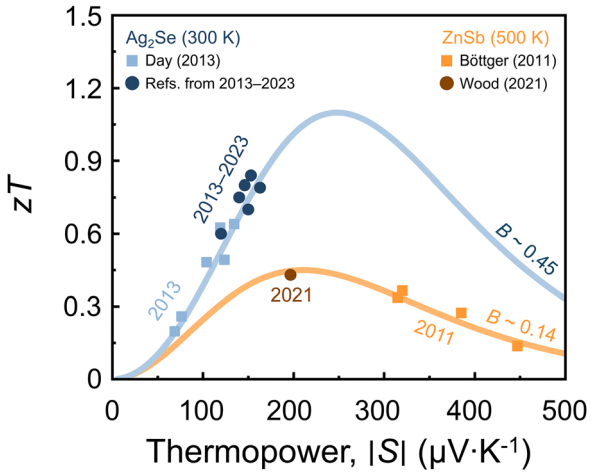

Fig. 4 Promising thermoelectric material candidates. In 2011, EM model analysis of Cu- or Sn-doped ZnSb predicted that tuning $|S|$ to 200 μV K^{-1} would yield a zT of ~0.45.[76] A decade later, increasing Sn doping within the Zn-rich phase space achieved zT = 0.43 by optimizing $|S|$ through defect control.[77] In 2013, experiments combined with EM model analysis predicted a zT of ~1.1, indicating that underdoping was needed to tune $|S|$.[78] Recently (~2023), $|S|$ ~ 163 μV K^{-1} was achieved, although further underdoping is still required to reach the optimum value.[79–84]

rapid, Hall effect-free determination of zT_{max}, the optimum $|S|$, and μ_w, while diagnosing whether performance is limited by doping, electronic structure, or scattering.

Applicable to degenerate and moderately non-degenerate semiconductors in which $|S|$ serves as a monotonic proxy for the reduced Fermi level and diffusion thermopower governs transport, the resulting zT expression (eqn (7)) functions as an effective transport descriptor, even when the material deviates from single parabolic band behaviour. In systems with multi-band contributions or band non-parabolicity, the extracted quantities should therefore be interpreted as effective transport parameters rather than strict band constants.

Applied to diverse systems, it captures band convergence, grain boundary effects, and defect-driven mobility changes, providing both mechanistic insight and quantitative performance targets. This broadly applicable approach can guide composition design, processing strategies, and practical implementation, accelerating the discovery and deployment of next-generation thermoelectric materials.

Author contributions

Conceptualization was done by G. J. Snyder, H. Kim, and M. Heo. M. Heo, K. H. Lee, and I. Lee developed the methodology. M. Heo, J. Song, C. Lee, and K. Kim conducted the investigation. J. Song and C. Lee were responsible for visualization. H. Wee and J. Lee acquired funding. I. Lee and K. Kim handled project administration. Y. Koh, H. Wee, and J. Lee supervised the project. The original draft was written by M. Heo, K. H. Lee, and J. Song. Y. Koh, H. Kim, and G. J. Snyder reviewed and edited the paper. The authors read, discussed, and commented on the manuscript.

Conflicts of interest

There are no conflicts to declare.

Data availability

All data supporting the findings of this study are available in the article and its supplementary information (SI). The SI includes additional derivations of the effective mass model and thermopower-based zT formulation, validation against the Hall-based EM model, weighted mobility analysis, and supporting figures and tables. See DOI: https://doi.org/10.1039/d5ee06413a.

Further information is available from the corresponding author on request.

Acknowledgements

This research was supported by Nano Material Technology Development Program through National Research Foundation of Korea (NRF) funded by the Ministry of Science and ICT (RS-2022-NR068194). This work was also supported by the National Research Foundation of Korea (NRF) grant funded by the Korea government (MSIT) (RS-2023-00212959).

Notes and references

1 J. Zhang, L. Song and B. B. Iversen, *npj Comput. Mater.*, 2019, **5**, 76.
2 C. J. Perez, M. Wood, F. Ricci, G. Yu, T. Vo, S. K. Bux, G. Hautier, G.-M. Rignanese, G. J. Snyder and S. M. Kauzlarich, *Sci. Adv.*, 2021, **7**, eabe9439.
3 Y. Pei, X. Shi, A. LaLonde, H. Wang, L. Chen and G. J. Snyder, *Nature*, 2011, **473**, 66–69.
4 X. Shi, S. Song, G. Gao and Z. Ren, *Science*, 2024, **384**, 757–762.
5 M. Y. Toriyama and G. J. Snyder, *Mater. Horiz.*, 2024, **11**, 1188–1198.
6 L. Hu, T. Zhu, X. Liu and X. Zhao, *Adv. Funct. Mater.*, 2014, **24**, 5211–5218.
7 J. Wang, H. Gao, K. Zhao, H. Wuliji, B. Zhao, J. Ma, X. Chen, J. Zhang, Y. Sui, T.-R. Wei, M. Zhu and X. Shi, *Sci. Adv.*, 2025, **11**, eadt6298.
8 Z.-Y. Huang, F. Wang, C. Jung, S. Zhang, F. Zu, C. Zhou and Y. Yu, *Mater. Today Phys.*, 2023, **37**, 101198.
9 S.-I. Kim, K. H. Lee, H. A. Mun, H.-S. Kim, S. W. Hwang, J. W. Roh, D. J. Yang, W. H. Shin, X. S. Li, Y. H. Lee, G. J. Snyder and S. W. Kim, *Science*, 2015, **348**, 109–114.
10 W. Ren, Y. Sun, D. Zhao, A. Aili, S. Zhang, C. Shi, J. Zhang, H. Geng, J. Zhang, L. Zhang, J. Xiao and R. Yang, *Sci. Adv.*, 2021, **7**, eabe0586.
11 S. Jia, H. Ma, S. Gao, L. Yang and Q. Sun, *Small*, 2024, **20**, 2405019.
12 S. Matern, S. V. Moreira, P. Samuelsson and M. Leijnse, *Phys. Rev. B*, 2024, **110**, 205423.

13 H. Zhou, T. Tian, X. Wang and J. Li, *Appl. Energy*, 2023, **332**, 120539.
14 B. M. Askerov, *Electron Transport Phenomena in Semiconductors*, World Scientific, Farrer Road, Singapore, 1994.
15 V. I. Fistul, *Heavily Doped Semiconductors*, Plenum Press, New York, NY, 1969.
16 A. F. Ioffe, L. S. Stil'bans, E. K. Iordanishvili, T. S. Stavitskaya, A. Gelbtuch and G. Vineyard, *Phys. Today*, 1959, **12**, 42.
17 A. J. Minnich, M. S. Dresselhaus, Z. F. Ren and G. Chen, *Energy Environ. Sci.*, 2009, **2**, 466–479.
18 Z. M. Gibbs, F. Ricci, G. Li, H. Zhu, K. Persson, G. Ceder, G. Hautier, A. Jain and G. J. Snyder, *npj Comput. Mater.*, 2017, **3**, 8.
19 S. Hao, L. Ward, Z. Luo, V. Ozolins, V. P. Dravid, M. G. Kanatzidis and C. Wolverton, *Chem. Mater.*, 2019, **31**, 3018–3024.
20 R. P. Chasmar and R. Stratton, *J. Electron. Control*, 1959, **7**, 52–72.
21 H. Wang, Y. Pei, A. D. LaLonde and G. J. Snyder, in *Thermoelectric Nanomaterials: Materials Design and Applications*, ed K. Koumoto and T. Mori, Springer Berlin Heidelberg, Berlin, Heidelberg, 2013, pp. 3–32.
22 S. D. Kang and G. J. Snyder, *arXiv*, 2018, preprint, arXiv:1710.06896, DOI: 10.48550/arXiv.1710.06896.
23 F. Werner, *J. Appl. Phys.*, 2017, **122**, 135306.
24 G. J. Snyder, A. Pereyra and R. Gurunathan, *Adv. Funct. Mater.*, 2022, **32**, 2112772.
25 H.-S. Kim, Z. M. Gibbs, Y. Tang, H. Wang and G. J. Snyder, *APL Mater.*, 2015, **3**, 041506.
26 G. J. Snyder, A. H. Snyder, M. Wood, R. Gurunathan, B. H. Snyder and C. Niu, *Adv. Mater.*, 2020, **32**, 2001537.
27 G. Jonker, *Philips Res. Rep.*, 1968, **23**, 131–138.
28 S. D. Kang and G. J. Snyder, *Nat. Mater.*, 2017, **16**, 252–257.
29 M. T. Agne, F. R. L. Lange, J. P. Male, K. S. Siegert, H. Volker, C. Poltorak, A. Poitz, T. Siegrist, S. Maier, G. J. Snyder and M. Wuttig, *Matter*, 2021, **4**, 2970–2984.
30 S. A. Gregory, R. Hanus, A. Atassi, J. M. Rinehart, J. P. Wooding, A. K. Menon, M. D. Losego, G. J. Snyder and S. K. Yee, *Nat. Mater.*, 2021, **20**, 1414–1421.
31 H. J. Goldsmid, in *Introduction to Thermoelectricity*, ed H. J. Goldsmid, Springer Berlin Heidelberg, Berlin, Heidelberg, 2016, pp. 45–66.
32 A. H. Wilson and J. Bardeen, *The Theory of Metals*, Cambridge Univ. Press, Cambridge, England, 1953.
33 A. F. May and G. J. Snyder, in *Materials, preparation, and characterization in thermoelectrics*, ed D. M. Rowe, CRC Press, Boca Raton, FL, 2012, pp. 1–18.
34 A. F. May, E. S. Toberer, A. Saramat and G. J. Snyder, *Phys. Rev. B: Condens. Matter Mater. Phys.*, 2009, **80**, 125205.
35 X. Zhang, Z. Bu, X. Shi, Z. Chen, S. Lin, B. Shan, M. Wood, A. H. Snyder, L. Chen, G. J. Snyder and Y. Pei, *Sci. Adv.*, 2020, **6**, eabc0726.
36 M. Cutler and N. F. Mott, *Phys. Rev.*, 1969, **181**, 1336–1340.
37 N. W. Ashcroft and N. D. Mermin, *Solid State Physics*, Holt, Rinehart and Winston, Boston, MA, 1976.
38 C. Kittel, *Introduction to Solid State Physics*, Wiley, Hoboken, NJ, 2011.
39 R. Hanus, R. Gurunathan, L. Lindsay, M. T. Agne, J. Shi, S. Graham and G. J. Snyder, *Appl. Phys. Rev.*, 2021, **8**, 031311.
40 E. S. Toberer, A. Zevalkink and G. J. Snyder, *J. Mater. Chem.*, 2011, **21**, 15843–15852.
41 C. Fanciulli, M. Codecasa, F. Passaretti and D. Vasilevskiy, *J. Electron. Mater.*, 2014, **43**, 2307–2313.
42 S. Whalen, S. Jana, D. Catalini, N. Overman and J. Sharp, *J. Electron. Mater.*, 2016, **45**, 3390–3399.
43 S. Y. Wang, W. J. Xie, H. Li, X. F. Tang and Q. J. Zhang, *J. Electron. Mater.*, 2011, **40**, 1150–1157.
44 W.-S. Liu, Q. Zhang, Y. Lan, S. Chen, X. Yan, Q. Zhang, H. Wang, D. Wang, G. Chen and Z. Ren, *Adv. Energy Mater.*, 2011, **1**, 577–587.
45 S. Ma, C. Li, L. Xing, X. Mu, W. Zhu, X. Nie, X. Sang, P. Wei, Q. Zhang and W. Zhao, *J. Electron. Mater.*, 2020, **49**, 2881–2889.
46 X. Duan, K. Hu, S. Ding, D. Man, W. Zhang and M. Ma, *Funct. Mater. Lett.*, 2015, **8**, 1550008.
47 Q. Lognoné and F. Gascoin, *J. Alloys Compd.*, 2015, **635**, 107–111.
48 L. D. Ivanova, L. I. Petrova, Y. V. Granatkina, V. S. Zemskov, O. B. Sokolov, S. Y. Skipidarov and N. I. Duvankov, *Inorg. Mater.*, 2009, **45**, 123–128.
49 X. Yan, B. Poudel, Y. Ma, W. S. Liu, G. Joshi, H. Wang, Y. Lan, D. Wang, G. Chen and Z. F. Ren, *Nano Lett.*, 2010, **10**, 3373–3378.
50 C. Kim, D. H. Kim, Y. S. Han, J. S. Chung, S. Park and H. Kim, *Powder Technol.*, 2011, **214**, 463–468.
51 W. Liu, K. C. Lukas, K. McEnaney, S. Lee, Q. Zhang, C. P. Opeil, G. Chen and Z. Ren, *Energy Environ. Sci.*, 2013, **6**, 552–560.
52 L. D. Ivanova, L. I. Petrova, Y. V. Granatkina, V. S. Zemskov, O. B. Sokolov, S. Y. Skipidarov, V. A. Kurganov and V. V. Podbel'skii, *Inorg. Mater.*, 2011, **47**, 459–464.
53 S. T. Han, P. Rimal, C. H. Lee, H.-S. Kim, Y. Sohn and S.-J. Hong, *Intermetallics*, 2016, **78**, 42–49.
54 K. C. Lukas, W. S. Liu, Z. F. Ren and C. P. Opeil, *J. Appl. Phys.*, 2012, **112**, 054509.
55 L. Cheng, Z.-G. Chen, L. Yang, G. Han, H.-Y. Xu, G. J. Snyder, G.-Q. Lu and J. Zou, *J. Phys. Chem. C*, 2013, **117**, 12458–12464.
56 X. Zhang and Y. Pei, *npj Quantum Mater.*, 2017, **2**, 68.
57 D. Zavanelli, A. Pröschel, J. Winograd, R. Cherkez and G. J. Snyder, *J. Appl. Phys.*, 2022, **131**, 115101.
58 G. J. Snyder and A. H. Snyder, *Energy Environ. Sci.*, 2017, **10**, 2280–2283.
59 N. H. Protik and B. Kozinsky, *Phys. Rev. B*, 2020, **102**, 245202.
60 R. Masuki, T. Nomoto and R. Arita, *Phys. Rev. B*, 2021, **103**, L041202.
61 H. J. Goldsmid and J. W. Sharp, *J. Electron. Mater.*, 1999, **28**, 869–872.
62 Z. M. Gibbs, H.-S. Kim, H. Wang and G. J. Snyder, *Appl. Phys. Lett.*, 2015, **106**, 022112.

63 M. Stordeur and W. Kühnberger, *Phys. Status Solidi B*, 1975, **69**, 377–387.
64 M. Stordeur, M. Stölzer, H. Sobotta and V. Riede, *Phys. Status Solidi B*, 1988, **150**, 165–176.
65 R. Sehr and L. R. Testardi, *J. Phys. Chem. Solids*, 1962, **23**, 1219–1224.
66 T. Plecháček, J. Navrátil, J. Horák and P. Lošťák, *Philos. Mag.*, 2004, **84**, 2217–2228.
67 M. K. Zhitinskaya, S. A. Nemov and T. E. Svechnikova, *Phys. Solid State*, 1998, **40**, 1297–1300.
68 Z. Su, J. He, X. Ji, N. Gothard and T. M. Tritt, *Sci. Adv. Mater.*, 2011, **3**, 596–601.
69 K. T. Kim, K. J. Kim and G. H. Ha, *Electron. Mater. Lett.*, 2010, **6**, 177–180.
70 H.-S. Kim, N. A. Heinz, Z. M. Gibbs, Y. Tang, S. D. Kang and G. J. Snyder, *Mater. Today*, 2017, **20**, 452–459.
71 O. Yamashita and S. Sugihara, *J. Mater. Sci.*, 2005, **40**, 6439–6444.
72 O. Yamashita, *Appl. Energy*, 2009, **86**, 1746–1756.
73 M. Wood, J. J. Kuo, K. Imasato and G. J. Snyder, *Adv. Mater.*, 2019, **31**, 1902337.
74 M. Ozen, A. B. Burcak, D. Zavanelli, M. Heo, M. Yahyaoglu, Y. Oz, U. Burkhardt, H.-S. Kim, G. J. Snyder and U. Aydemir, *ACS Appl. Mater. Interfaces*, 2024, **16**, 52501–52514.
75 S. Zhan, T. Hong, B. Qin, Y. Zhu, X. Feng, L. Su, H. Shi, H. Liang, Q. Zhang, X. Gao, Z.-H. Ge, L. Zheng, D. Wang and L.-D. Zhao, *Nat. Commun.*, 2022, **13**, 5937.
76 P. H. M. Böttger, G. S. Pomrehn, G. J. Snyder and T. G. Finstad, *Phys. Status Solidi A*, 2011, **208**, 2753–2759.
77 M. Wood, M. Y. Toriyama, S. Dugar, J. Male, S. Anand, V. Stevanović and G. J. Snyder, *Adv. Energy Mater.*, 2021, **11**, 2100181.
78 T. Day, F. Drymiotis, T. Zhang, D. Rhodes, X. Shi, L. Chen and G. J. Snyder, *J. Mater. Chem. C*, 2013, **1**, 7568–7573.
79 W. Mi, P. Qiu, T. Zhang, Y. Lv, X. Shi and L. Chen, *Appl. Phys. Lett.*, 2014, **104**, 133903.
80 K. H. Lim, K. W. Wong, Y. Liu, Y. Zhang, D. Cadavid, A. Cabot and K. M. Ng, *J. Mater. Chem. C*, 2019, **7**, 2646–2652.
81 H. Wang, W. Chu, D. Wang, W. Mao, W. Pan, Y. Guo, Y. Xiong and H. Jin, *J. Electron. Mater.*, 2011, **40**, 624–628.
82 S. Y. Tee, X. Y. Tan, X. Wang, C. J. J. Lee, K. Y. Win, X. P. Ni, S. L. Teo, D. H. L. Seng, Y. Tanaka and M.-Y. Han, *Inorg. Chem.*, 2022, **61**, 6451–6458.
83 M. Jin, J. Liang, P. Qiu, H. Huang, Z. Yue, L. Zhou, R. Li, L. Chen and X. Shi, *J. Phys. Chem. Lett.*, 2021, **12**, 8246–8255.
84 J. Chen, Q. Sun, D. Bao, T. Liu, W.-D. Liu, C. Liu, J. Tang, D. Zhou, L. Yang and Z.-G. Chen, *ACS Appl. Mater. Interfaces*, 2020, **12**, 51523–51529.

